Penetration of Surfactin into Phospholipid Monolayers: Nanoscale Interfacial Organization

M. Eeman,† A. Berquand,‡ Y. F. Dufrêne,‡ M. Paquot,† S. Dufour,† and M. Deleu*,†

Unité de Chimie Biologique Industrielle, Faculté Universitaire des Sciences Agronomiques de Gembloux, Passage des Déportés, 2, B-5030 Gembloux, Belgium, and Unité de Chimie des Interfaces, Université Catholique de Louvain, Croix du Sud 2/18, B-1348 Louvain-la-Neuve, Belgium

Received July 7, 2006. In Final Form: September 19, 2006

Atomic force microscopy (AFM) combined with surface pressure−area isotherms were used to probe the interfacial behavior of phospholipid monolayers following penetration of surfactin, a cyclic lipopeptide produced by *Bacillus subtilis* strains. Prior to penetration experiments, interfacial behavior of different surfactin molecules (cyclic surfactins with three different aliphatic chain lengths—S13, S14, and S15—and a linear surfactin obtained by chemical cleavage of the cycle of the surfactin S15) has been investigated. A more hydrophobic aliphatic chain induces greater surface-active properties of the lipopeptide. The opening of the peptide ring reduces the surface activity. The effect of phospholipid acyl chain length (dimyristoylphosphatidylcholine, dipalmitoylphosphatidylcholine− (DPPC), and distearoylphosphatidylcholine) and phospholipid polar head (DPPC, dipalmitoylphosphatidylethanolamine and dipalmitoylphosphatidylserine) on monolayer penetration properties of the surfactin S15 has been explored. Results showed that while the lipid monolayer thickness and the presence of electrostatic repulsions from the interfacial film do not significantly influence surfactin insertion, these parameters strongly modulate the ability of the surfactin to alter the nanoscale organization of the lipid films. We also probed the effect of surfactin structure (influence of the aliphatic chain length and of the cyclic structure of the peptide ring) on the behavior of DPPC monolayers. AFM images and isotherms showed that surfactin penetration is promoted by longer lipopeptide chain length and a cyclic polar head. This indicates that hydrophobic interactions are of main importance for the penetration power of surfactin molecules.

Introduction

Surfactins are lipopeptides produced by several *Bacillus subtilis* strains. They are composed of a heptapeptide cycle linked to a β-hydroxy fatty acid chain (Figure 1A).[1] Surfactins exhibit strong surface activity and important biological properties, including antiviral, antibacterial, and haemolytic activities.[2−4] The biological activity of surfactins relies on their interactions with biomembranes.

One way to study such interactions is to evaluate their ability to penetrate model membranes, in particular, lipid monolayers. The advantages of such bidimensional model systems are that they are flat, homogeneous, and stable. They also offer the possibility to simulate what happens when an active molecule, soluble in extracellular medium, interacts with the membrane of the target cells.[5] The penetration of insoluble monolayers by a soluble amphiphile (surfactant and protein) has been extensively studied to understand the biological effects of such molecules at the membrane level.[6−12] In most studies, fluorescence microscopy or Brewster angle microscopy were used to visualize the evolution of the surfactant insertion into the monolayer and the subsequent changes of the interfacial behavior. The latter technique presents the advantage of not using a fluorescent probe that may result in domain instability for highly compressed monolayers.[13] These optical techniques offer a lateral resolution in the micrometer range and are thus not suited to visualize the phase properties of lipid monolayers at high resolution. In this context, atomic force microscopy (AFM) is an important probing technique since one can view lipid domains in phase-separated films with nanometer scale resolution.[14−19]

A. Cyclic surfactin

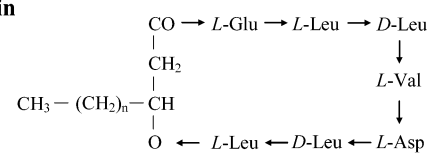

B. Linear surfactin

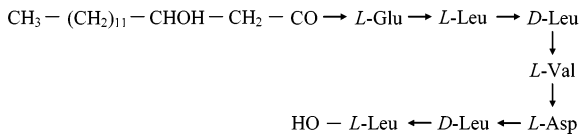

Figure 1. Primary structures of (A) cyclic surfactin ($n = 9$, 10, and 11, respectively, for surfactin with a β-hydroxy fatty acid chain of 13, 14, and 15 carbon atoms) and (B) linear surfactin (β-hydroxy fatty acid chain of 15 carbon atoms).

* Corresponding author. Phone: (32) 81 62 22 32. Fax: (32) 81 62 22 31. E-mail: deleu.m@fsagx.ac.be.

† Unité de Chimie Biologique Industrielle.

‡ Université Catholique de Louvain.

(1) Kakinuma, A.; Ouchida, A.; Shima, T.; Sugino, H.; Isono, H.; Tumara, G.; Arima, K. *Agric. Biol. Chem.* **1969**, *33*, 1669.

(2) Bernheimer, A. W.; Avigad, L. S. *J. Gen. Microbiol.* **1970**, *61*, 361.

(3) Vollenbroich, D.; Özel, M.; Vater, J.; Kamp, R. M.; Pauli, G. *Biologicals* **1997**, *25*, 289.

(4) Vollenbroich, D.; Pauli, G.; Özel, M.; Vater, J. *Appl. Env. Microbiol.* **1997**, *63*, 44.

(5) Maget-Dana, R. *Biochim. Biophys. Acta* **1999**, *1462*, 109.

(6) Bougis, P.; Rochat, H.; Pieroni, G.; Verger, R. *Biochemistry* **1981**, *20*, 4915.

(7) Bos, M. A.; Nylander, T. *Langmuir* **1996**, *12*, 2791.

(8) Gonzales-Christen, J.; Vergne, I.; Süβmuth, R.; Sidobre, S.; Prats, M.; Tocanne, J. F.; Lanéelle, G. *Biochim. Biophys. Acta* **1998**, *1368*, 97.

(9) Fainerman, V. B.; Zhao, J.; Vollhardt, D.; Makievski, A. V.; Li., J. B. *J. Phys. Chem. B* **1999**, *103*, 8998.

(10) Sun, Y.-T.; Wang, S.-X.; Sui, S.-F. *Colloids Surf., A* **2000**, *175*, 105.

(11) Zhao, J.; Vollhardt, D.; Brezesinski, G.; Siegel, S.; Wu, J.; Li, J. B.; Miller, R. *Colloids Surf., A* **2000**, *171*, 175.

(12) Xicohtencatl-Cortes, J.; Mas-Oliva, J.; Castillo, R. *J. Phys. Chem. B* **2004**, *108*, 7307.

(13) McConlongue, C. W.; Vanderlick, T. K. *Langmuir* **1997**, *13*, 7158.

10.1021/la061969p CCC: $33.50
Published on Web 10/31/2006

In this paper, AFM is combined with the Langmuir trough technique to study the incorporation of surfactin into lipid monolayers, which are transferred onto a solid support by the Langmuir−Blodgett (LB) technique after surfactin penetration. Maget-Dana and Ptak have already shown that surfactins penetrate differently into lipid layers according to the charge and chain length of the lipids.[20] In contrast to their work, in the present study, we use physiological conditions (Tris 10 mM, NaCl 150 mM, pH 7.2) to better mimic the biological situation. Moreover, the association of data from AFM analysis (domain formation, step height, and friction images) and surface pressure evolution as a function of time (maximal surface pressure and exclusion pressure) gives more information about the surfactin penetration behavior (bulk diffusion and monolayer penetration) as well as their conformational arrangement at the interface. The influence of the fatty acid chain length and nature of the polar head of surfactin on its penetration power into lipid membranes is also investigated.

Materials and Methods

Materials. Surfactin molecules with a β-hydroxy fatty acid chain of 13 (S13), 14 (S14), and 15 (S15) carbon atoms (molecular weights, 1007.7, 1021.7, and 1035.7, respectively) were used in this study (Figure 1A). They were produced and purified as previously described.[21] Their isolation from crude surfactins was performed by preparative reversed-phase chromatography using a Waters 5 μm Atlantis C_{18} column (1.9 cm × 10 cm, Waters, Milford, MA) and a acetonitrile/water/trifluoroacetic acid 0.1% mixture as the mobile phase. The primary structure and purity (>95%) of surfactins were ascertained by analytical reversed-phase high-performance liquid chromatography, amino acid analysis,[22] and Maldi-Tof mass spectrometry measurements (Ultraflex TOF, Bruckner, Karlsruhe, Germany).

Surfactin S15L was obtained by chemical cleavage of the heptapeptide cycle from the natural surfactin S15 (Figure 1B). The cleavage of this lactone ring leading to the linearization of the surfactin was carried out by dissolving the natural molecule in 8 mL of methanol and 12 mL of sodium hydroxide 0.1 M and by heating this solution at 37 °C for approximately 20 h.[23,24]

1,2-Dimyristoyl-*sn*-glycerol-3-phosphocholine (DMPC); 1,2-dipalmitoyl-*sn*-glycerol-3-phosphocholine (DPPC); 1,2-distearoyl-*sn*-glycerol-3-phosphocholine (DSPC); 1,2-dipalmitoyl-*sn*-glycerol-3-phosphoethanolamine (DPPE); and 1,2-dipalmitoyl-*sn*-glycerol-3-phospho-L-serine (DPPS) were purchased from Avanti Polar Lipids (Alabaster, AL).

Monolayer Studies. For isotherm experiments, pure surfactin monolayers were prepared at 20 ± 0.2 °C with an automated LB system (KSV minitrough: area 24225 mm^2, KSV instruments Ltd., Helsinki, Finland). Surfactins were dissolved at 1 mM in chloroform/methanol (2:1). An aliquot (30 μL) was spread on a Tris/NaCl 10:150 mM (Millipore Co., Milford, MA) subphase adjusted at pH 7.2 with HCl. After evaporation of the solvent (15 min), monolayers were compressed at a rate of 10 mm/min with a two symmetrical barriers system. The surface pressure of the lipid monolayer was measured using a platinum plate with an accuracy of 0.1 mN/m. The difference between molecular areas of two independent sets of measurements was less than 5%.

For adsorption experiments, the same system was used. The adsorption area was delimited by the two barriers and corresponded to the same effective area as the one used in the penetration experiments. Injection of surfactin molecules, solubilized in dimethyl sulfoxide (99.90% A.C.S. Reagent, Sigma), in the subphase (final concentration of 5.3 10^{-7} M) was operated using a setup ensuring them to be homogeneously and reproducibly distributed. The syringe was placed in the clean interface compartment, and a long bent needle going below the barrier was displaced carefully and uniformly all over the subphase supporting the monolayer. After the injection of surfactin, the increase in surface pressure was recorded.

For the penetration experiments, lipid monolayers were prepared in the same conditions and with the same LB system as stated previously. Expanded monolayers were compressed at a defined initial surface pressure. As soon as the initial surface pressure was stabilized (~20 min), surfactin, solubilized in dimethyl sulfoxide, was injected into the subphase to a final concentration of 5.3×10^{-7} M using the same injection setup as described previously. When the surface pressure reached a maximal value, the monolayer was stabilized at this pressure and deposited by vertically raising freshly cleaved mica (width: 10 mm and− height: 15 mm) through the air−water interface at a rate of 10 mm/min. The transfer ratios were all approximately 1:1, confirming that AFM images were representative of the trough interface. Pure dimethyl sulfoxide injections into the subphase did not modify the initial surface pressure of phospholipid monolayers.

AFM Measurements. AFM measurements were performed at room temperature (20 °C) using a commercial optical lever microscope (Nanoscope III, Digital Instruments, Santa Barbara, CA). Contact mode topography and friction images were recorded using oxide-sharpened microfabricated Si_3N_4 cantilevers (Park Scientific Instruments, Mountain View, CA) with a typical radius curvature of 20 nm and spring constants around 0.01 N/m. Scan rates ranging from 3 to 5 Hz were tested. The applied force was maintained as low as possible during the imaging.

Results and Discussion

Prior to penetration experiments, the interfacial behavior of different surfactin molecules (natural cyclic surfactins with three different aliphatic chain lengths—S13, S14, and S15—and a linear surfactin obtained by chemical cleavage of the cycle from natural surfactin S15, S15L) has been investigated.

Surface Pressure−Area ($\pi - A$) Isotherms of Surfactins. Figure 2A shows the surface pressure−area ($\pi - A$) isotherms, at the air−water interface, of pure surfactin monolayers. Both the natural cyclic surfactins (S13, S14, and S15) and the linear surfactin (S15L) present a $\pi - A$ isotherm with a sigmoidal shape. No sharp increase of the surface pressure is observed at very low areas per molecule, while it was revealed for a surfactin monolayer formed on a water subphase acidified at pH 2.[25] Maget-Dana and Ptak have also shown that at pH > 4, the sharp increase of the surface pressure does not exist even at low temperatures,[26,27] and they have suggested that the ionization of the glutamic and aspartic residues favors the interaction of surfactin molecules with the subphase preventing their perpendicular orientation to the interface. Despite the presence of Na^+ cations in our experiments, which are susceptible to screen the negative charges of surfactin, there is not a sharp increase of surface pressure at low molecular area. The main difference between the isotherms

(14) Dufrêne, Y. F.; Barger, W. R.; Green, J.-B. D.; Lee, G. U. *Langmuir* **1997**, *13*, 4779.
(15) Vié, V.; Van Mau, N.; Chaloin, L.; Lesniewska, E.; Le Grimellec, C.; Heitz, F. *Biophys. J.* **2000**, *78*, 846.
(16) Giocondi, M.-C.; Vié, V.; Lesniewska, E.; Milhiet, P. E.; Zinke-Allmang, M.; Le Grimellec, C. *Langmuir* **2001**, *17*, 1653.
(17) Yuan, C.; Johnston, L. J. *Biophys. J.* **2002**, *79*, 2768.
(18) Deshayes, S.; Plénat, T.; Aldrian-Herrada, G.; Divita, G.; Le Grimellec, C.; Heitz, F. *Biochemistry* **2004**, *43*, 7698.
(19) Eeman, M.; Deleu, M.; Paquot, M.; Thonart, P.; Dufrêne, Y. F. *Langmuir* **2005**, *21*, 2505.
(20) Maget-Dana, R.; Ptak, M. *Biophys. J.* **1995**, *68*, 1937.
(21) Razafindralambo, H.; Paquot, M.; Hbid, C.; Jacques, P.; Destain, J.; Thonart, P. *J. Chromatogr.* **1993**, *639*, 81.
(22) Moore, S.; Stein, W. *J. Biol. Chem.* **1951**, *192*, 663.
(23) Morikawa, M.; Hirata, Y.; Imanaka, T. *Biochim. Biophys. Acta* **2000**, *1488*, 211.
(24) Dufour, S.; Deleu, M.; Nott, K.; Wathelet, B.; Thonart, P.; Paquot, M. *Biochim. Biophys. Acta* **2005**, *1726*, 87.
(25) Deleu, M.; Paquot, M.; Jacques, P.; Thonart, P.; Adriaensen, Y.; Dufrêne, Y. F. *Biophys. J.* **1999**, *77*, 2304.
(26) Maget-Dana, R.; Ptak, M. *J. Colloid Interface Sci.* **1992**, *153*, 285.
(27) Maget-Dana, R.; Ptak, M. *Thin Solid Films* **1992**, *210/211*, 730.

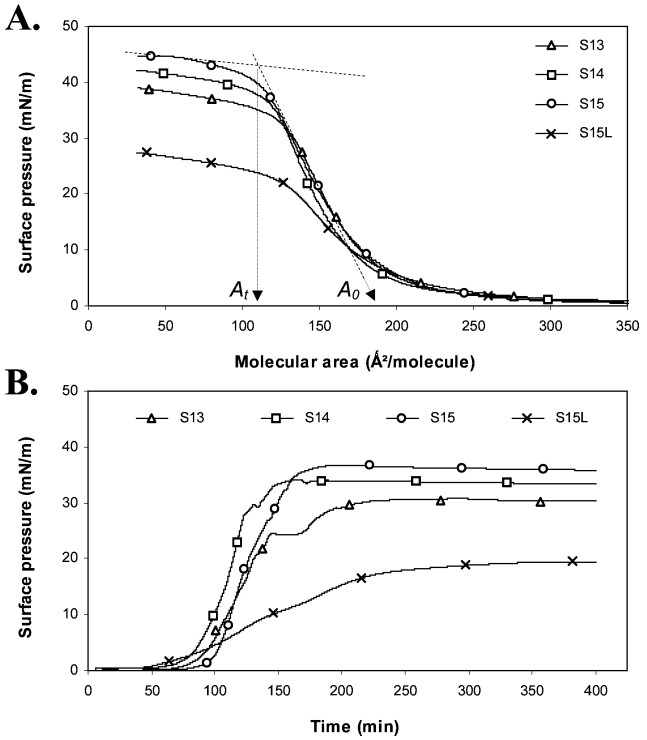

Figure 2. (A) Surface pressure−area ($\pi - A$) isotherms, at the air−water interface (10 mM Tris/150 mM NaCl; pH 7.2; 20 °C) of pure surfactin monolayers. A_0: Limiting area (extrapolation of the $\pi - A$ plot to $\pi = 0$ mN/m). This parameter corresponds to the theoretical area at which molecules leave the gaseous state and adopt a liquid-expanded state. A_t: Area of the intersection point between the tangents to the two parts of the $\pi - A$ curve (see the dashed lines). (B) Surface pressure increase vs time to the injection of surfactin in the subphase. Surfactin concentration in the subphase: 5.3×10^{-7} M. Injection at time zero.

of S13, S14, S15, and S15L is the maximum surface pressure under compression. A more hydrophobic alkyl chain induces a higher surface pressure ($\pi_{A = 35\ Å^2/\text{molecule}} = 38.9$, 42.0, and 44.7 mN/m for S13, S14 and S15, respectively) and consequently greater surface-active properties of the lipopeptide. However, for the same chain length, the opening of the peptide ring reduces the maximal surface pressure and therefore the surface activity of surfactin ($\pi_{A = 35\ Å^2/\text{molecule}} = 27.4$ mN/m for S15L vs 44.7 mN/m for S15). Nevertheless, the area occupied by the molecule during the compression is only slightly influenced by the nature of the polar head (limiting area: $A_0 = 190$ and 202 Å^2/molecule and area at transition pressure: $A_t = 110$ and 123 Å^2/molecule for S15 and S15L, respectively).

Adsorption of Surfactins at the Air−Water Interface. The adsorption of surfactin molecules at a clean interface is revealed by the increase in surface pressure as a function of time (Figure 2B). Each cyclic molecule (S13, S14, and S15) takes more than 50 min after its injection in the subphase to start to significantly modify the surface pressure value, originally equal to 0 mN/m. Moreover, the extrapolation of their surface concentration Γ (calculated from the compression isotherm data[28]) to a zero value does not intercept the *X*-axis at time zero (Figure 3A−C, closed symbols). Delay time in both surface pressure increase and surface concentration increase indicates that natural cyclic surfactins do not adsorb immediately at the interface when they are injected in the bulk solution. This is in contradiction with results of Razafindralambo et al. who have shown a rapid adsorption of surfactin at the air−water interface.[29] The very low bulk

(28) Maget-Dana, R.; Ptak, M. *Colloids Surf., B* **1996**, *7*, 135.

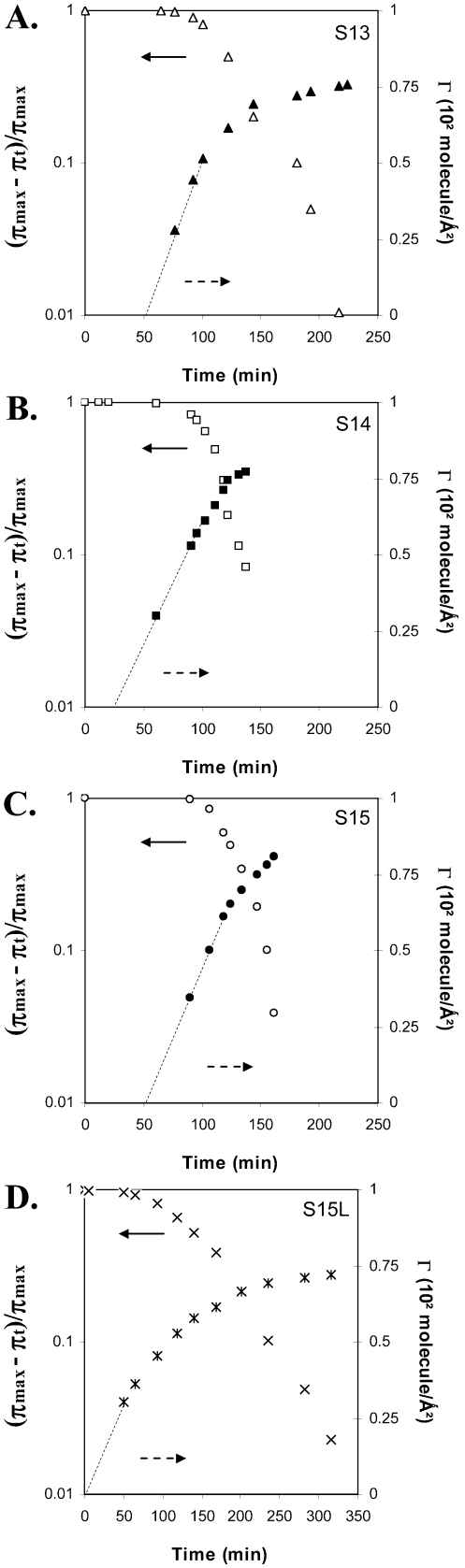

Figure 3. (A−D) Kinetic plot according to eq 1 and time dependence of surfactin surface concentration Γ.

concentration and the large interfacial area in our Langmuir trough experiment in comparison with those of their dynamic surface tension measurements are the main reasons for the discrepancy. After this first slow diffusion step, the lipopeptide molecules rapidly adsorb and organize at the interface as suggested by the

abrupt increase of surface pressure and surface concentration values. These observations are in accordance with the adsorption kinetics determined by the following first-order equation:

$$\ln[(\pi_{max} - \pi_t)/(\pi_{max} - \pi_0)] = -Kt \quad (1)$$

where π_{max}, π_t, and π_0 are the surface pressure values at the plateau, at time t, and at time zero, respectively, and K is the rate constant. The plots obtained for cyclic surfactins (Figure 3A−C, opened symbols) show two distinct areas, both of them being characterized by a specific rate constant (K_1 and K_2). As already evoked by Maget-Dana and Ptak for the globular protein defensin A, K_2 reflects the interfacial rearrangement following the molecules' adsorption.[28] Cyclic surfactins present rather high K_2 values (45×10^{-2} min^{-1} for S13 and 57×10^{-2} min^{-1} for S14 and S15), indicating that the interfacial organization of these compounds is very fast. This phenomenon can be explained by the rigid conformation of cyclic surfactins, which reduces their degree of freedom at the interface. The maximum surface pressure values obtained for different cyclic surfactins are reached between 150 and 250 min after their injection in the subphase (Figure 2B). Cyclic surfactins with longer fatty acid chains induce higher surface pressures, indicating that a more hydrophobic chain favors a better conformational stability of the adsorbed molecules (π_{max} = 30.8, 34.2, and 36.8 mN/m for S13, S14, and S15, respectively). The same trend was also observed by Razafindralambo et al. with dynamic surface tension measurements.[29] Indeed, they have shown that the surface tension values obtained after equilibrium decrease with increasing hydrophobic character of the surfactin alkyl chain (γ_{CMC} = 36.4, 33.5, and 31.9 mN/m for S13, S14, and S15, respectively).

The adsorption process of the linear surfactin is initiated before the adsorption of the cyclic lipopeptide. Indeed, S15L needs approximately half the time to induce a significant increase of the surface pressure than its cyclic analogue (∼40 min for S15L vs ∼80 min for S15) (Figure 2B). The higher mobility of the molecule due to the opening of the peptide cycle could contribute to the highest diffusion up to the interface. Graham and Phillips have reported in the case of proteins that the surface pressure increase is more rapid for flexible molecules than rigid and globular molecules.[30] The cleavage of the cyclic polar head also alters the interfacial stability of the surfactin since the maximum surface pressure value resulting in the lipopeptide adsorption is notably reduced (19.5 mN/m for S15L vs 36.8 mN/m for S15). The plot of the calculated surface concentration Γ of linear surfactin as a function of time can be extrapolated to zero without discontinuity (Figure 3D, closed cross). It shows that this molecule diffuses directly up to the interface after its injection in the subphase. Once at the interface, several results indicate that its interfacial rearrangement is slower than cyclic surfactin. First, the slope of the π − time curve of S15L is less abrupt than the one of S15 (Figure 2B). Second, the plateau in surface pressure is only reached after ∼300 min (as compared to ∼200 min in the case of S15). Finally, the adsorption kinetics of S15L (Figure 3D, opened cross) presents a much lower K_2 value (17×10^{-2} min^{-1} for S15L vs 57×10^{-2} min^{-1} for S15). Both the slower rearrangement and the lower stability of linear surfactin at an air−water interface can be explained by the presence of an extra negative charge with the linearization of the peptide cycle, which accentuates the surfactin affinity for the aqueous subphase.

Penetration Experiments. The influence of both phospholipid nature (chain length and polar head charge) and surfactin structure

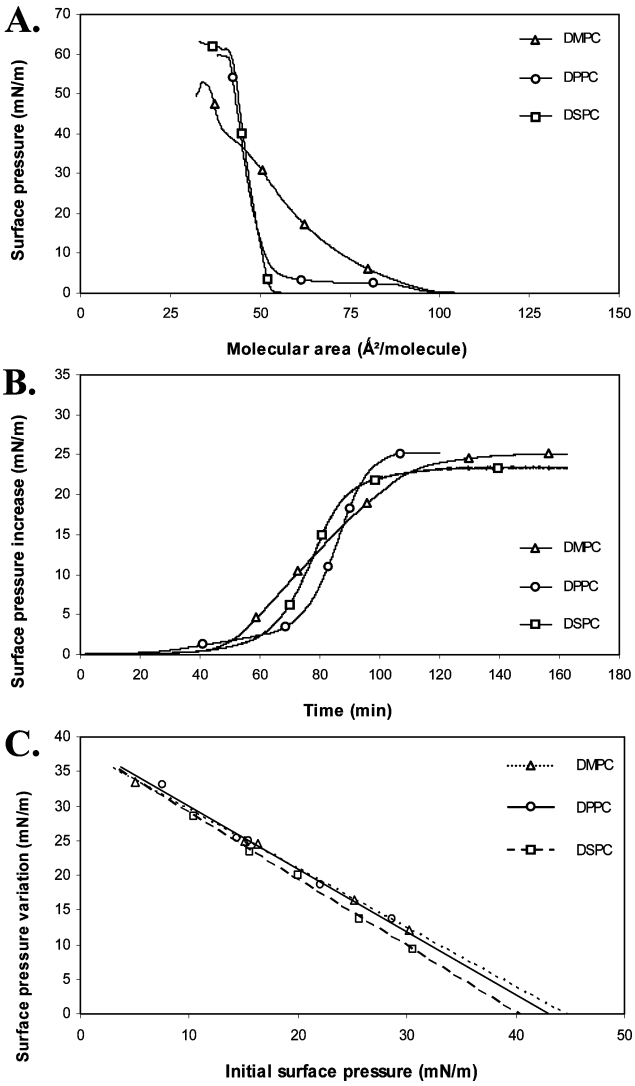

Figure 4. (A) Surface pressure−area (π − A) isotherms, at the air−water interface of pure DMPC, DPPC, and DSPC monolayers. (B) Penetration kinetics of surfactin S15 into DMPC, DPPC, and DSPC monolayers (π_i = 15 mN/m). (C) Surface pressure increase as a function of the initial pressure of these lipid monolayers.

(chain length and peptide structure) on the penetration of surfactin into phospholipid monolayers has been investigated at the nanometer scale.

Effect of the Phospholipid Chain Length. DMPC, DPPC, and DSPC were used to investigate the ability of surfactin S15 to penetrate into a lipid monolayer differing only by the phospholipid chain length. These three polar lipids have two saturated chains with 14, 16, and 18 carbon atoms, respectively. According to the π − A isotherm (Figure 4A) and in accordance with the literature,[31−35] DMPC molecules are in a homogeneous liquid-expanded state at 15 mN/m (i.e., the surface pressure at which surfactin is injected beneath the lipid monolayer) and, consequently, do not adopt a very compact organization. For the same initial surface pressure, DPPC and DSPC monolayers are not homogeneous. AFM images (data not shown) show clearly

(29) Razafindralambo, H.; Thonart, P.; Paquot, M. *J. Surfactants Deterg.* **2004**, *7*, 41.
(30) Graham, D. E.; Phillips, M. C. *J. Colloid Interface Sci*. **1979**, *70*, 403.
(31) Phillips, M. C.; Chapman, D. *Biochim. Biophys. Acta* **1986**, *163*, 301.
(32) Shapovalov, V. L.; Kotova, E. A.; Rokitskaya, T. I.; Antonenko, Y. N. *Biophys. J.* **1999**, *77*, 299.
(33) Bordi, F.; Cametti, C.; De Luca, F.; Gili, T.; Gaudino, D.; Sennato, S. *Colloids Surf., B* **2003**, *29*, 149.
(34) Zhao, L. Y.; Feng, S. S. *J. Colloid Interface Sci.* **2004**, *274*, 55.
(35) Matsumoto, M.; Tsujii, Y.; Nakamura, K. I.; Yoshimoto, T. *Thin Solid Films* **2005**, *280*, 238.

Table 1. Surfactin Penetration in Phospholipid Monolayers[a]

no.	phospholipid monolayer	surfactin	regression line	R^{2b}	$\pi_c{}^c$ (mN/m)	$\pi_m{}^d$ (mN/m)	$\Delta h^e \pm 0.1$ nm
A	DMPC	S15	$y = -0.8553x + 38.025$	0.9988	44.5	40.9	0.9
	DPPC	S15	$y = -0.9073x + 39.093$	0.9913	43.1	42.4	1.2
	DSPC	S15	$y = -0.9583x + 38.533$	0.9972	40.2	40	1.4
B	DPPC	S15	$y = -0.9073x + 39.093$	0.9913	43.1	42.4	1.2
	DPPE	S15	$y = -0.8665x + 37.221$	0.9903	43.0	39.9	0.8
	DPPS	S15	$y = -0.9967x + 38.950$	0.9987	39.1	40.6	0.9
C	DPPC	S13	$y = -0.9522x + 33.574$	0.9973	35.3	33.9	0.7
	DPPC	S14	$y = -0.9179x + 35.628$	0.9993	38.8	37.8	0.9
	DPPC	S15	$y = -0.9073x + 39.093$	0.9913	43.1	42.4	1.2
	DPPC	S15L	$y = -1.0291x + 25.925$	0.9987	25.2	24.7	0.9

[a] A: Effect of the phospholipid chain length. B: Effect of the phospholipid polar head. C: Effect of surfactin alkyl chain and polar head. [b] R^2: Determination coefficients of regression lines. [c] π_e: Exclusion pressure. [d] π_m: Transfer pressure. [e] Δh: Step height between the two phases obtained from three cross-sections from three different AFM topography images.

a phase separation that can be attributed to the coexistence of a few remaining liquid-expanded domains dispersed into a liquid-condensed matrix. The monolayers are thus mainly in a liquid-condensed state, and the orientation of the phospholipid acyl chains may be considered as almost vertical.

Kinetic plots (Figure 4B) show three finite regions. The first corresponds to the plateau at 0 mN/m before a significant increase in surface pressure. It characterizes the diffusion time of surfactin up to the interface. For the three phospholipid monolayers, this time is similar ($t_{\Delta\pi = 1.0\ \mathrm{mN/m}} \approx 40$ min), meaning that surfactin diffusion does not depend on the phospholipid chain length. The second region corresponding to the linear increase of surface pressure with time characterizes the actual penetration of surfactin into the lipid monolayer. The slope of this linear part reflects the kinetics of the penetration process, a higher slope corresponding to a faster penetration. Surprisingly, the penetration kinetics of surfactin is slower when the interfacial film is composed of DMPC (Figure 4B). The insertion of surfactin into an unordered DMPC monolayer probably modifies the orientation of the phospholipid. This mutual rearrangement is slow and can explain the weaker increase of surface pressure induced by surfactin penetration. On the contrary, surfactin penetration in more tightly packed phosphatidylcholine monolayers (DPPC and DSPC) and its subsequent interfacial organization can be achieved more rapidly without greatly perturbing the configuration of the phospholipid molecules. The few liquid-expanded domains of phospholipids remaining in the monolayer may be preferential sites for surfactin insertion but do not affect highly its kinetic penetration.

The final plateau at a constant surface pressure corresponds to the third region of the penetration kinetics (Figure 4B) and characterizes a steady state. By plotting the surface pressure increase ($\Delta\pi$) as a function of the initial surface pressure (π_i) of the lipid monolayer, the exclusion pressure is determined (π_e: extrapolation of the regression line to a surface pressure increase equal to zero) (Figure 4C).[6,20] This parameter corresponds to the initial surface pressure of the phospholipid monolayer above which no more surfactin molecules can penetrate the lipid film and increase the surface pressure. π_e reflects the penetration power of surfactin into the lipid monolayers. The exclusion pressure values obtained for the three phospholipids decrease weakly with an increase of the phospholipid chain length ($\pi_e =$ 44.5, 43.1, and 40.2 mN/m for DMPC, DPPC, and DSPC, respectively) (Figure 4C). The lateral order into the lipid monolayer influences the penetration power of surfactin. The better the order is, the lower the penetration power.

When the surfactin penetration profile reached a steady-state surface pressure (π_m), the mixed surfactin−phospholipid monolayer was transferred onto a solid support (see Table 1A for the transfer surface pressure, π_m) and analyzed by AFM. In the case of surfactin−DMPC monolayer, the AFM image shows phase separation ($\Delta h = 0.9 \pm 0.1$ nm) (Figure 5A). As the transfer pressure ($\pi_m = 40.9$ mN/m) corresponds for the pure DMPC monolayer to the end of the transition between the liquid-expanded and the liquid-condensed states (Figure 4A), most DMPC molecules should be in a vertical, compact organization. The pure DMPC monolayer transferred at 40.9 mN/m demonstrated that this is not the case as the AFM topography image is not homogeneous but also reveals phase separation (data not shown). At 40.9 mN/m, pure surfactin does not form a condensed state in the investigated conditions. Surfactin molecules are rather in a loose organization with a not well-defined orientation. They are thus more likely to form domains with a lower height than well-organized regions of phospholipids. In agreement with the uniform AFM images obtained for a preformed surfactin−DMPC monolayer at 20 mN/m (below the LE−LC transition) (data not yet published), we suggest that surfactin coexists with less-ordered DMPC molecules. This indicates that the lighter domains and the darker matrix in Figure 5A probably correspond to well-organized vertical DMPC molecules and to less-ordered DMPC molecules mixed with surfactin, respectively. However, complete

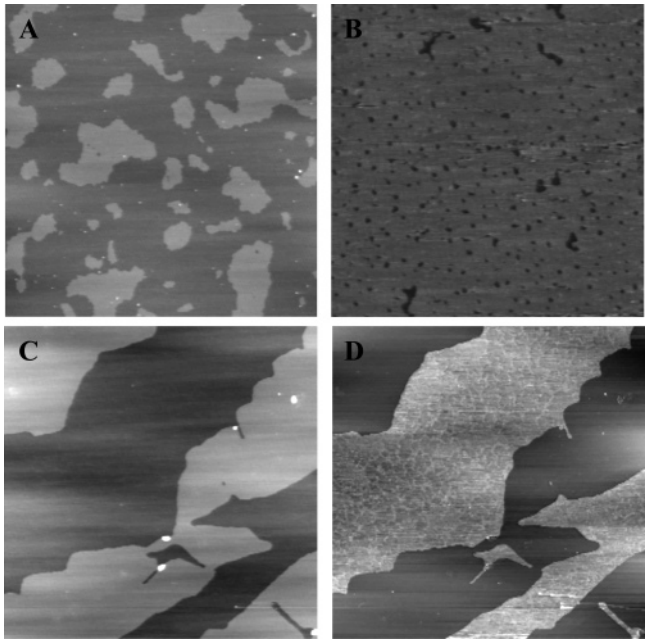

Figure 5. Effect of the phospholipid chain length on the organization of mixed surfactin/phospholipid monolayers. AFM height (A and B) (*Z*-range: 3 nm) and friction (C) (*Z*-range: 0.2 V) images of mixed films obtained after penetration of surfactin S15 in phospholipid monolayers (A: DMPC; B: DPPC; and C and D: DSPC), initially compressed at 20 mN/m. The image size is 5 μm × 5 μm (A and B) and 10 μm × 10 μm (C and D). Lighter levels in the images correspond to higher height and higher friction.

miscibility between the two components cannot be confirmed because these loosely organized molecules are susceptible to be flattened by the AFM probe and will therefore not be able to display height differences.

The AFM topography image for the surfactin−DPPC film (Figure 5B) exhibits phase separation in the form of small irregular aggregates embedded in a continuous matrix. If we assume that all DPPC molecules are in a solid state (i.e., in a vertical orientation) at the transfer pressure ($\pi_m = 42.4$ mN/m), the lighter matrix (higher level) can be attributed to DPPC domains and the lower level (darker regions) to the surfactin-enriched phase.

The AFM image for the surfactin−DSPC films shows phase separation in the form of large domains embedded in a continuous matrix (Figure 5C). If we assume that all DSPC molecules are in a solid state and consequently adopt a tight vertical organization, the higher level can be attributed to a phospholipid-enriched phase. Moreover, the step height between the two phases ($\Delta h = 1.4 \pm 0.1$ nm) is similar to the value obtained when the phospholipid is spread at the interface in a surfactin mixture ($\Delta h = 1.3 \pm 0.1$ nm for a premixed surfactin/DSPC monolayer: data not yet published). The friction image provides further information about the nature of the phases. Gray and black zones in the friction image (Figure 5D) correspond to dark and light zones in the topography image, respectively (Figure 5C). While black zones in the friction image are uniform, the gray zones are not. Regions of higher friction and lower height are thus composed of a mixture of molecules adopting different states of compaction. It could be a mixture of surfactin molecules with a part of them in a liquid-expanded state (more flexible) and the other part in a transition state (more rigid) or a mixture of surfactin in a liquid-expanded state and DSPC molecules in a pseudo-solid state. To test these hypotheses, the observed surface coverage of surfactin and its theoretical surface coverage can be compared. The theoretical surface coverage of surfactin (TSC) is calculated by use of the following equations:

$$\mathrm{TSC} = \frac{A_S}{A_L} 100 \tag{2}$$

with

$$A_S = A_L - A_{PPL} \tag{3}$$

$$A_{PPL} = A_{DSPC} N_{DSPC} \tag{4}$$

$$N_{DSPC} = \frac{N_{DSPC} V_{DSPC} N_A}{M_w} \tag{5}$$

where A_S, A_L, A_{PPL}, and A_{DSPC} are the total area occupied by surfactin after its penetration into a DSPC monolayer, the available area of the Langmuir trough, the total area occupied by DSPC molecules spread at the interface, and the mean molecular area occupied by DSPC at the transfer pressure (using compression isotherm data), respectively. N_{DSPC} is the number of phospholipid molecules spread at the interface. C_{DSPC}, V_{DSPC}, N_A, and M_w are the concentration and the volume of the DSPC solution that is spread at the interface, Avogadro's constant, and the molecular weight of DSPC, respectively.

The theoretical surface coverage of surfactin (TSC) is close to 14% and thus much smaller than the observed surface coverage of dark zones (about 50% of the surface). It means that the dark zones in the topography image are occupied by surfactin and DSPC molecules.

Taken together, these results show that the penetration power of surfactin and the nanoscale organization of the interfacial components are more sensitive to the lateral arrangement of the phospholipids than to their chain length.

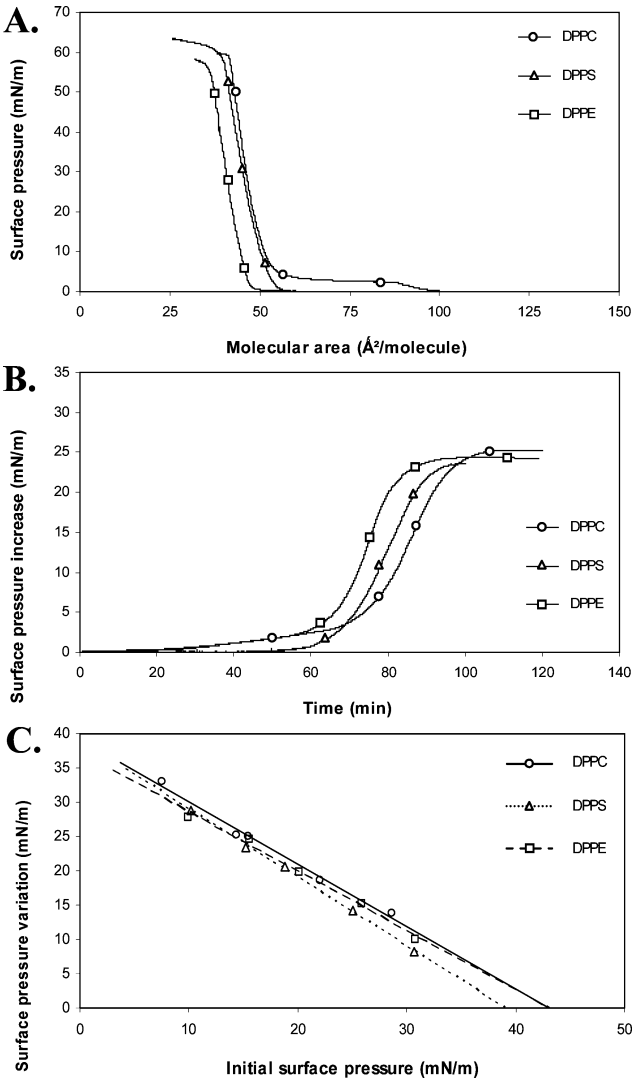

Figure 6. (A) Surface pressure−area ($\pi - A$) isotherms, at the air−water interface of pure DPPC, DPPE, and DPPS monolayers. (B) Penetration kinetics of surfactin S15 into DPPC, DPPE, and DPPS monolayers ($\pi_i = 15$ mN/m). (C) Surface pressure increase as a function of the initial pressure of these lipid monolayers.

Effect of the Phospholipid Polar Head. DPPC, DPPE, and DPPS were used to study the ability of surfactin S15 to insert into a lipid monolayer differing only by the phospholipid polar head. These three polar lipids have two saturated chains with 16 carbon atoms. At pH 7.2, the headgroup of DPPC and DPPE bears a positive and a negative charge. However, the steric hindrance is less important for the DPPE molecules. At the same pH, DPPS has two negative and one positive charge. The presence of Na^+ ions in the subphase may screen the negative charges of both DPPS and surfactin, which bears also two negative charges at the investigated pH. Before the injection of surfactin in the subphase ($\pi_i = 15$ mN/m), the three phospholipid monolayers are mainly in a liquid-condensed state (Figure 6A).

Kinetic plots analysis (Figure 6B) shows that the diffusion time of surfactin to the interface (first region of the kinetic plots) is delayed when the lipid monolayer is charged ($t_{\Delta\pi = 1.0\ \mathrm{mN/m}} \approx$ 40 min for DPPC and DPPE and $t_{\Delta\pi = 1.0\ \mathrm{mN/m}} \approx 65$ min for DPPS). This suggests that electrostatic repulsions still exist despite the presence of Na^+ cations in the subphase. Hence, the shielding of negative charges of both surfactin and DPPS by Na^+

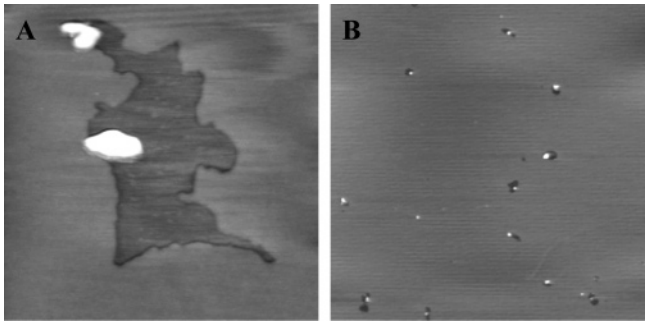

Figure 7. Effect of the phospholipid polar head on the organization of mixed surfactin/phospholipid monolayers. AFM height images (*Z*-range: 3 nm and image size: 5 μm × 5 μm) of mixed films obtained after penetration of surfactin S15 in phospholipid monolayers (A: DPPS and B: DPPE), initially compressed at 20 mN/m. Lighter levels in the images correspond to higher height.

cations is not complete. This correlates with the difference between exclusion pressures of zwitterionic and negatively charged monolayers (π_e = 43.1, 43.0, and 39.1 mN/m for DPPC, DPPE, and DPPS, respectively) (Figure 6C), meaning that surfactin has a higher penetration power in an uncharged monolayer than a charged one. Nevertheless, this difference is much smaller than the one reported by Maget-Dana and Ptak,[20] who used DMPC and DMPE as zwitterionic phospholipids ($\pi_e \approx 40$ mN/m) and bovine brain phosphatidylserine as a negatively charged phospholipid ($\pi_e \approx 14$ mN/m) and a subphase without Na^+. Other studies have also shown that an increase in ionic strength by added NaCl partially shields the surface potential of negatively charged model membranes.[7,36−38]

The kinetic of the penetration process is not influenced by the polar head nature of phospholipids as reflected by the similar slopes of the linear part (second region of the kinetic plots) for the three monolayers.

Figure 7 shows the nanoscale interfacial organization of surfactin−DPPE and surfactin−DPPS monolayers transferred at the steady-state surface pressure π_m (see Table 1B) on a mica support (LB technique) after surfactin penetration. In the case of surfactin−DPPS, a phase separation is observed (Figure 7A). On the basis of another study (data not yet published) on a premixed surfactin/DPPS monolayer (AFM study), we attribute the lower level to surfactin-enriched domains and the lighter one to a phospholipid-enriched matrix. This strong immiscibility between the two interfacial components is in agreement with molecular modeling data[39] showing a more favorable self-association of surfactin than its interaction with DPPS.

The smaller, lighter domains, protruding around 1.3 nm above the homogeneous matrix, were also detected in all independent preparations. Their regular borders and their specific location on top of the surfactin-enriched domains suggest that they are multilayers of surfactin rather than impurities. However, it is well-known that AFM images of LB films transferred from a NaCl-containing aqueous subphase reveal usually square domains (50−100 nm) of lighter contrast corresponding to NaCl crystals.[40] Such aggregates were also found in some of our preparations but are different from the lighter domains observed in the AFM images presented in this paper.

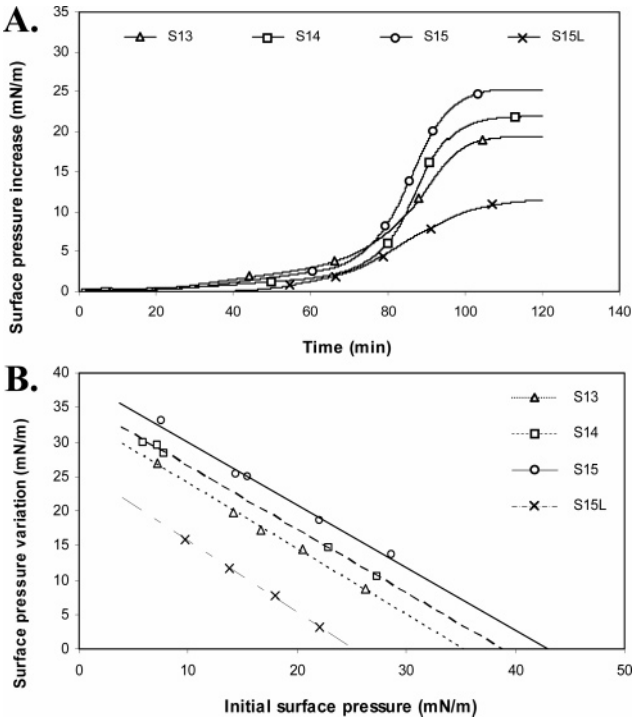

Figure 8. (A) Surface pressure increase vs time related to surfactin penetration into a DPPC monolayer initially compressed at 15 mN/m. (B) Surface pressure increase vs the initial pressure of a DPPC monolayer. Surfactin concentration in the subphase: 5.3×10^{-7} M. Injection at time zero.

An AFM image of surfactin−DPPE system shows some small, deep domains flanked by light spots and surrounded by a uniformly higher matrix (Figure 7B). Considering the previous results, domains can be suggested to be surfactin and spots to be surfactin multilayers. Comparison of the surface coverage of the lower domains with the theoretical value (eqs 2−5) shows that the uniform matrix is not only composed of phospholipids but probably corresponds to a DPPE-rich phase including some surfactin molecules. This means that specific interactions between surfactin and DPPE are created. Conformational accommodations between the cone-shape of DPPE and the inverted cone-shape of surfactin[41] as well as the ability of both DPPE[42−45] and surfactin[46,47] polar heads to form, respectively, inter- and intramolecular hydrogen bonds lead us to believe that specific interactions such as hydrogen bonding could also exist between PE and surfactin molecules.

Effect of Surfactin Alkyl Chain and Polar Head. A DPPC monolayer was used to investigate the penetration properties of both cyclic (S13, S14, and S15) and linear (S15L) surfactin molecules. Penetration profiles (Figure 8A) are identical (sigmoidal shape) for all cyclic molecules, and the required time for observing a significant increase of surface pressure is quite similar ($t_{\Delta\pi = 1.0\ mN/m} \approx 40$ min). This is shorter than the one in the absence of lipid films (Figure 2B), suggesting that the presence of a lipid film at the air−water interface favors cyclic surfactin diffusion. As for the adsorption experiment, cyclic surfactins

(36) Hauser, H.; Shipley, G. G. *Biochemistry* **1983**, *22*, 2171.
(37) Agasøsler, A. V.; Tungodden, L. M.; Èejka, D.; Bakstad, E.; Sydnes, L. K.; Holmsen, H. *Biochem. Pharmacol.* **2001**, *61*, 817.
(38) Quinn, P. J.; Dawson, M. C. *Biochem. J.* **1969**, *115*, 65.
(39) Deleu, M.; Bouffioux, O.; Razafindralambo, H.; Paquot, M.; Hbid, C.; Thonart, P.; Jacques, P.; Brasseur, R. *Langmuir* **2003**, *19*, 3377.
(40) Van Mau, N.; Vié, V.; Chaloin, L.; Lesniewska, E.; Heitz, F.; Le Grimellec, C. *J. Membr. Biol.* **1999**, *167*, 241.
(41) Chernomordik, L. *Chem. Phys. Lipids* **1996**, *81*, 203.
(42) Boggs, J. M. *Biochim. Biophys. Acta* **1987**, *906*, 353.
(43) Sen, A., Yang, P. W.; Mantsch, H. H.; Hui, S.-W. *Chem. Phys. Lipids* **1988**, *47*, 109.
(44) Seddon, J. M. *Biochim. Biophys. Acta* **1990**, *1031*, 1.
(45) Pink, D. A.; McNeil, S.; Quinn, B.; Zuckermann, M. J. *Biochim. Biophys. Acta* **1998**, *1368*, 289.
(46) Bonmatin, J.-M.; Genest, M.; Labbé, H.; Ptak, M. *Biopolymers* **1994**, *34*, 975.
(47) Nicolas, J. P. *Biophys. J.* **2003**, *85*, 1377.

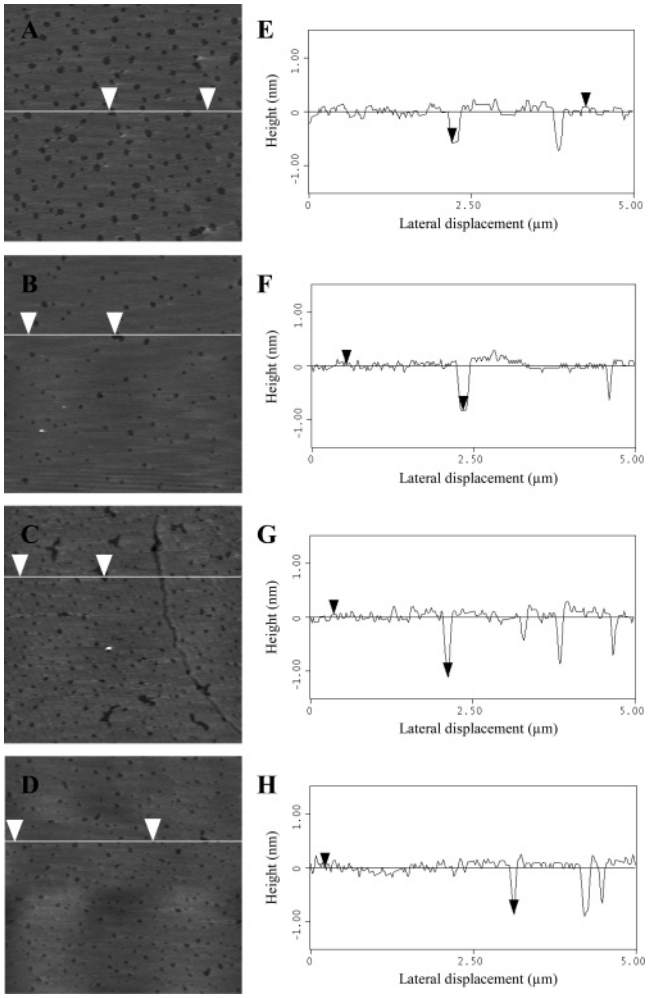

Figure 9. Effect of the surfactin nature on the organization of mixed surfactin/DPPC monolayers. (A−D) AFM height images (*Z*-range: 3 nm and image size: 5 μm × 5 μm) of mixed films obtained after surfactin penetration (A: S13; B: S14; C: S15; and D: S15L) in a DPPC monolayer, initially compressed at 20 mN/m. Lighter levels in the images correspond to higher height. (E−H) Section analysis obtained from the images (white line) (E: S13; F: S14; G: S15; and H: S15L).

with longer fatty acid chains induce higher surface pressures.

The surface pressure increase ($\Delta\pi$) versus initial surface pressure (π_i) plots show that, whatever the initial surface pressure of the DPPC monolayer, lipopeptides with longer fatty acid chains induce a higher surface pressure increase (Figure 8A). Consequently, the more hydrophobic the surfactin, the higher the exclusion pressure (π_e = 35.3, 38.8, and 43.1 mN/m for S13, S14, and S15, respectively) (Figure 8B).

The shallower slope of the $\Delta\pi$ − time curve in the case of S15L as compared with S15 suggests that linear surfactin is slower to incorporate into a DPPC monolayer than cyclic surfactin (Figure 8A). The lower penetration of linear surfactin into model membranes is confirmed by the lower surface pressure increase induced. This is in accordance with the significantly lower exclusion pressure displayed by the linear molecule (π_e = 25.2 mN/m for S15L vs 43.1 mN/m for S15) (Figure 8B).

The mixed surfactin−DPPC films were stabilized at the maximal surface pressure (π_m: Table 1C) before being transferred for AFM analysis. The AFM topography images obtained for the cyclic surfactin/DPPC systems (Figure 9A−C) show phase separations in the form of small irregular aggregates embedded in a continuous matrix. On the basis of the above results, lower and higher levels can be attributed to surfactin- and DPPC-enriched phases, respectively. Surprisingly, the step height between the domains increases with increasing lipopeptide chain length (Δh = 0.7, 0.9, and 1.2 ± 0.1 nm for systems involving S13, S14, and S15, respectively) (Figure 9E−G). If we assume that the average height of the DPPC-enriched phase remains constant after surfactin insertion, differences in step height can be attributed to surfactin conformation changes. In this case, the surfactin with a longer alkyl chain should present a lower step height with respect to DPPC. Our results show the opposite trend. In accordance with the study of Gallet et al.[48] using a molecular modeling approach, we suggest a folding of a surfactin fatty acid chain on the peptide ring. This folding is probably governed by hydrophobic interactions between the aliphatic chain and the hydrophobic amino acids of the surfactin cycle as this effect is more pronounced for longer lipopeptide chains. Such molecular arrangements can explain the better conformational stability of the more hydrophobic surfactins when they adsorb at an air−water interface.

The alteration of DPPC molecule arrangements into DPPC richer regions by insertion of surfactin could also be assumed. In this case, a perturbation of their tight packing and, consequently, a modification of their vertical orientation could explain the higher step height observed. However, Deleu et al.[39] have shown that surfactin prefers to self-associate than to interact with phospholipids. Another study (data not yet published) has also shown that only the borders of DPPC-rich regions comprise surfactin molecules. The average height of the domains is then not significantly affected.

The AFM topography image obtained after penetration of the linear surfactin into a DPPC monolayer shows a similar phase separation to the one observed with natural cyclic surfactin (Figure 9C,D). The step height between surfactin- and DPPC-enriched phases, however, decreases notably when the peptide cycle is linearized despite having the same number of carbon atoms in the lipid chain (Δh = 0.9 ± 0.1 for S15L vs 1.2 ± 0.1 nm for S15) (Figure 9G,H). If we assume that the change of surfactin structure does not affect DPPC arrangement, the step height results together with the slight difference of interfacial molecular area suggest that linear and cyclic molecules adopt different conformations at the interface. Both the interfacial arrangement of the linear peptide moiety and the folding of the fatty acid chain could be affected by the linearization of the peptide cycle. The more hydrophilic nature of the linear molecule, due to the existence of an extra hydroxyl group on the fatty acid chain, may reduce intramolecular hydrophobic interactions and consequently the folding of the fatty acid chain.

In summary, surfactin insertion into a DPPC monolayer strongly depends on both the lipopeptide chain length and the nature of the surfactin polar head.

Conclusion

This paper shows that the combined use of AFM and the Langmuir trough technique is a valuable approach to investigate the penetration of lipopeptides into phospholipid monolayers and their nanoscale organization.

Maget-Dana and Ptak[20] have shown that insertion of a surfactin into a lipid monolayer becomes more difficult when the phospholipid chain length increases. According to them, the presence of a negative charge on the phospholipid polar head gives rise to electrostatic repulsions, preventing the peptide cycle from coming close to the phospholipid headgroups.

(48) Gallet, X.; Deleu, M.; Razafindralambo, H.; Jacques, P.; Thonart, P.; Paquot, M.; Brasseur, R. *Langmuir* **1999**, *15*, 2409.

Our study provides insight as to the influence of the phospholipid nature (chain length and polar head charge) on surfactin penetration into a lipid monolayer by exploring the nanoscale organization at the interface. This highlights the added importance of surfactin structure on its membrane insertion properties. Moreover, this study gives valuable insight into molecular conformations of surfactin within a lipid matrix.

Although the length of phospholipid acyl chains (DMPC, DPPC, and DSPC) does not have a significant influence on the ability of surfactin to insert in a phosphatidylcholine monolayer, it modulates the ability of surfactin to perturb the nanoscale interfacial organization of the preexistent phospholipid monolayer differently.

The surfactin penetration is not significantly affected by the presence of electrostatic repulsions in the phospholipid monolayer (DPPS) and by the size of the polar headgroup (DPPE and DPPC). The addition of Na^+ ions in the subphase inhibits the charge effect during the penetration process as also evoked by Maget-Dana and Ptak[20] for Ca^{2+} ions. The presence of salt may also decrease the electrostatic repulsion between the adsorbed molecules and consequently favor hydrophobic interactions.[49] This suggests that in the presence of salt, the penetration process is mainly governed by hydrophobic interactions between the fatty acid chain of surfactin and the phospholipid chains. However, the topography AFM images obtained for these systems indicate that the presence of a negative net charge in the phospholipid monolayer promotes the immiscibility between the interfacial components.

The length of the lipopeptide chain and the nature of the peptide moiety influence both surfactin adsorption onto a monolayer free interface and surfactin penetration into a lipid film. On the basis of changes to surface pressure and exclusion pressure values, we conclude that the longer the surfactin acyl chain, the better its insertion into the lipid layer. This indicates that hydrophobic interactions are of main importance for the penetration power of surfactin. The presence of a cyclic polar head (in contrast with a linear one) also favors the surfactin penetration into a DPPC monolayer.

In light of these results, we suggest that linear surfactin mainly adopts a random coil conformation in the subphase, favoring a faster diffusion to the interface. However, once at the interface, cyclic molecules with a rigid conformation have a reduced degree of freedom, making their interfacial rearrangement very rapid. At the interface, cyclic surfactins most likely adopt a conformation in which the fatty acid chain is folded on the peptide ring. This folding is governed by the increased intramolecular hydrophobic interactions with lipopeptide chain length. The delocalization of the additional OH function on the linear surfactin as compared to those of the glutamic and aspartic residues reduces the amphiphilic character of surfactin and consequently its surface activity and penetration power into lipid membranes.

All the results provide new information about the interaction of surfactin with biological membranes. First, in physiological conditions, surfactin is able to penetrate into cellular membranes independently of their phospholipid nature (π_e is higher than the estimated lateral pressure of natural bilayers,[50] which is comprised between 30 and 35 mN/m). The cyclic nature of the peptide moiety as well as the fatty acid chain length play a considerable role in the lipopeptide activity. Second, negatively charged phospholipids promote immiscibility of surfactin into the lipid matrix. They are thus in favor of surfactin self-assembly formation, which is the basis of pore-forming activity. For this reason, we suggest that surfactin, as for other antimicrobial peptides,[51] exhibits a target selectivity behavior based on the composition of the lipid matrix of the target cell. In particular, the lipopeptide could display a high pore-forming activity for membranes with a considerably high amount of anionic lipids, such as bacterial membranes, aged blood erythrocytes, and some cancer cells.

In future studies, it would be interesting to investigate the penetration of surfactin in more complex model monolayers incorporating other important lipids of cell membranes such as cholesterol and sphingomyelin, which are involved in lipid raft formation in biological membranes.[52] Other techniques such as quartz crystal microbalance with dissipation monitoring (QCM-D) and isothermal titration calorimetry (ITC) could be also very useful to quantify the interactions between surfactin and such model membranes.

Acknowledgment. M.D. and Y.F.D. are Research Associates of the National Foundation for Scientific Research (F.N.R.S.). The support of the Région Wallonne (021/5103) and of the F.N.R.S. is gratefully acknowledged. The authors thank Prof. P. Thonart and his team (Unité de Bio-industries, Faculté Universitaire des Sciences Agronomiques de Gembloux, Belgium) for the production of the surfactin by fermentation of the *Bacillus subtilis* strain S499. The authors thank Sam Edgecombe (Department of Physical Chemistry 1, Lund University, Sweden) warmly for his critical reading of the manuscript.

LA061969P

(49) Miller, I. R.; Bach, D. *Chem. Phys. Lipids* **1974**, *13*, 453.

(50) Marsh, D. *Biochim. Biophys. Acta* **1996**, *1286*, 183.

(51) Willumeit, R.; Kumpudgee, M.; Funari, S. S.; Lohner, K.; Navas, B. P.; Bradenburg, K.; Linser, S.; Andrä, J. *Biochim. Biophys. Acta* **2005**, *1669*, 125.

(52) Simons, K.; Ikonen, E. *Nature* **1997**, *387*, 569.